

Evolution of porous dust grains in protoplanetary discs – I. Growing grains

A. J. L. Garcia,¹[★] and J.-F. Gonzalez,¹[†]

¹Univ Lyon, Univ Claude Bernard Lyon 1, Ens de Lyon, CNRS, Centre de Recherche Astrophysique de Lyon UMR5574, F-69230, Saint-Genis-Laval, France

Accepted 2020 February 6. Received 2020 February 6; in original form 2019 April 29

ABSTRACT

One of the main problems in planet formation, hampering the growth of small dust to planetesimals, is the so-called radial-drift barrier. Pebbles of cm to dm sizes are thought to drift radially across protoplanetary discs faster than they can grow to larger sizes, and thus to be lost to the star. To overcome this barrier, drift has to be slowed down or stopped, or growth needs to be sped up. In this paper, we investigate the role of porosity on both drift and growth. We have developed a model for porosity evolution during grain growth and applied it to numerical simulations of protoplanetary discs. We find that growth is faster for porous grains, enabling them to transition to the Stokes drag regime, decouple from the gas, and survive the radial-drift barrier. Direct formation of small planetesimals from porous dust is possible over large areas of the disc.

Key words: Protoplanetary discs - Hydrodynamics - Planets and satellites: formation - Methods: numerical

1 INTRODUCTION

In protoplanetary discs, planetesimals are thought to be the building blocks of planets (Safronov 1972). However, our understanding of the collisional growth of sub-micron-sized monomers up to kilometre-sized planetesimals is hindered by problems called ‘barriers’ in the planet formation theory. Because of the gas pressure gradient, a differential velocity exists between gas and dust, and grains experience an aerodynamic drag force. Grains thus lose angular momentum, making them settle down to the mid-plane and drift inwards. The influence of the drag force can be measured by the Stokes number St , i.e. the ratio between the grain stopping time (the time for a grain to reach the gas velocity) to the Keplerian orbital time. Small grains, with $St \ll 1$, and large grains, with $St \gg 1$, are respectively very coupled with the gas and weakly affected by the gas drag and so, drift slowly. Grains with intermediate sizes, i.e. $St \sim 1$, are subject to the fastest radial drift. Thus, initially small grains growing to this intermediate regime can be accreted onto the star faster than they can grow to reach planetesimal sizes (Adachi et al. 1976; Weidenschilling 1977). To overcome this barrier, called the “radial-drift barrier”, grain growth needs to be accelerated or drift slowed down. So-called dust traps have been shown to be a good way to slow down drift by accumulating grains in a gas pressure maximum (Haghighipour 2005) such as, e.g., in vortices (Barge & Sommeria 1995; Meheut et al. 2012; Zhu et al. 2014), snow lines (Kretke & Lin 2007; Brauer et al. 2008; Drążkowska

& Alibert 2017) or planet gaps (Paardekooper & Mellema 2004; Fouchet et al. 2007, 2010; Ayliffe et al. 2012; Pinilla et al. 2012; Zhu et al. 2012, 2014). More recently, Gonzalez et al. (2017a,b) showed that self-induced dust traps can form without an initially present pressure maximum in the disc, where growing and fragmenting grains can accumulate thanks to the combined effect of the back-reaction of dust on gas and large-scale gradients.

In this work, we choose to investigate on the growth of porous grains as a solution. Indeed, at a given mass, porous grains have a larger collisional cross-section than compact dust, which can accelerate growth. Until now, grains have been considered as compact in most studies of grain growth (e.g. Brauer et al. 2008; Laibe et al. 2008; Drążkowska et al. 2014; Gonzalez et al. 2015a), for the sake of simplicity and because of a lack of knowledge on how porosity evolves with collisions. However, some objects in the Solar system such as comets have appeared to be porous (Blum et al. 2006; A’Hearn 2011; Sierks et al. 2015). Experiments have also shown that low-velocity collisions lead to the formation of porous aggregates (Blum 2004). Furthermore, experimental and numerical works have studied faster collisions and found that collisional energy is dissipated by internal restructuring and that compression can occur (Dominik & Tielens 1997; Blum & Wurm 2000; Wada et al. 2007, 2008, 2009; Suyama et al. 2008, 2012; Seizinger et al. 2012). The importance of porosity on the collisional evolution of dust grains, and in particular its ability to assist growth, was first evidenced in numerical simulations by Ormel et al. (2007). Based on the numerical model of evolution of porosity during collisions of Suyama et al. (2008), Okuzumi et al. (2012) then investigated the formation of icy planetesimals from direct growth of porous aggre-

★ E-mail: anthony.garcia@ens-lyon.fr

† E-mail: jean-francois.gonzalez@ens-lyon.fr

Table 1. Parameters of our disc models. Values with subscript 0 are given for $R_0 = 1$ AU.

Model	p	q	R_{in} (AU)	R_{out} (AU)	R_{esc} (AU)	$T_{\text{g},0}$ (K)	$\Sigma_{\text{g},0}$ ($\text{kg}\cdot\text{m}^{-2}$)
CTTS	3/2	3/4	3	300	400	197	4537
Flat	0	1	4	120	160	619	11

gates and found that porosity can help grains overcome the radial-drift barrier. However, in their study, planetesimals have a density lower than $10^{-3} \text{ kg m}^{-3}$, inconsistent with comet values. Kataoka et al. (2013b) thus introduced the static compression process to take into account restructuring due to gas or self-gravity compression. As it is difficult and impractical to treat at the same time the evolution of porosity during collisions at small scales and the disc physics at large scales, studies including porosity have mostly been carried out in a local context, i.e. at a given distance from the star (Ormel et al. 2007; Okuzumi et al. 2009; Kataoka et al. 2013b). However, Okuzumi et al. (2012) and Krijt et al. (2016) computed the radial evolution of grain mass and porosity in a 1D disc model. In this paper, in order to link both the small and large scales, we derive a model of porosity evolution to reproduce the effects of collisions and include it in global 3D simulations of dust growth and dynamics.

We detail our models for growth and porosity as well as our numerical codes in Section 2. In Section 3, we present our results on the influence of porosity on growth and drift and we discuss on how porosity can be a solution to the radial-drift barrier in Section 4. We summarise our work and conclude in Section 5.

2 METHODS

2.1 Disc models

We simulate a disc of mass $M_{\text{disc}} = 0.01 M_{\odot}$ around a $1 M_{\odot}$ star. Initially, the dust-to-gas ratio by mass ϵ , defined as the ratio between dust and gas local volume densities $\rho_{\text{d}}/\rho_{\text{g}}$, is taken to be 0.01. We model the disc as power laws of the distance from the star R . Thus, the gas surface density scales as $\Sigma_{\text{g}} \propto R^{-p}$ and its temperature as $T_{\text{g}} \propto R^{-q}$. In all simulations, we use a constant Shakura & Sunyaev (1973) α parameter of 10^{-2} . The disc extends from R_{in} to R_{out} . We assume that dust moving outside of a distance R_{esc} or inside R_{in} is respectively escaped or accreted into the star.

We consider two disc models characterised by two different disc geometries: a disc around a classical T-Tauri star (CTTS) (studied by, e.g., Barrière-Fouchet et al. 2005; Laibe et al. 2008) and a ‘‘Flat’’ disc, a simple model with a constant surface density (used in, e.g., Paardekooper & Mellema 2004; Fouchet et al. 2007; Gonzalez et al. 2015a). Both models correspond to different outcomes regarding the radial-drift barrier for non-growing grains according to Laibe et al. (2012): dust grains are expected to survive the barrier in the CTTS disc but not in the Flat disc. We study both in this work to examine whether porosity impacts this behaviour. The different parameters of those disc are given in Table 1.

2.2 Drag regimes and drift

The differential velocity between gas and dust creates an aerodynamic friction. Grains are in different drag regimes according to

how their size s compares to the mean free path of gas molecules λ . Stepinski & Valageas (1996) give the expression of the gas dynamical viscosity as a function of λ as

$$\mu_{\text{g}} = \frac{1}{2} \rho_{\text{g}} \lambda c_{\text{g}}, \quad (1)$$

where

$$c_{\text{g}} = \sqrt{\frac{k_{\text{B}} T_{\text{g}}}{m_{\text{g}}}} \quad (2)$$

is the gas sound speed, with m_{g} the mean gas molecule mass. This yields

$$\lambda = \frac{2\mu_{\text{g}}}{\rho_{\text{g}} c_{\text{g}}}. \quad (3)$$

The Chapman-Enskog theory provides a refined calculation of μ_{g} . In the Sutherland model, which describes rigid elastic spheres with weak mutual attraction, it can be approximated as

$$\mu_{\text{g}} = \frac{5\sqrt{\pi} m_{\text{g}} c_{\text{g}}}{64 \sigma_{\text{mol}}} \quad (4)$$

(Chapman & Cowling 1970), where $\sigma_{\text{mol}} = 2 \times 10^{-19} \text{ m}^2$ is the cross-section of the H_2 molecule, and we take $m_{\text{g}} = 2.32 m_{\text{H}} = 3.883038752 \times 10^{-27} \text{ kg}$. When $s < 9\lambda/4$, the grain is in the Epstein drag regime (Epstein 1924) and when $s > 9\lambda/4$, it is in the Stokes regime (Whipple 1972). In those regimes, the grain’s Stokes number can be expressed as

$$\text{St} = \begin{cases} \frac{\rho_{\text{s}} \phi s}{\rho_{\text{g}} c_{\text{g}}} \Omega_{\text{K}}, & \text{(Epstein)} \\ \frac{2\rho_{\text{s}} \phi s^2}{9\mu_{\text{g}}} \Omega_{\text{K}}, & \text{(Stokes)} \end{cases} \quad (5)$$

where ρ_{s} is the bulk density of the grain and Ω_{K} is the Keplerian angular velocity. ϕ is the grain filling factor and will be discussed in Section 2.4. Note that some authors use the gas sound speed while others use the mean thermal velocity of gas molecules in the calculation of the drag force in the Epstein regime. We use the former. The resulting expressions for St differ by a factor $\sqrt{\pi}/8$, of order unity. In the Stokes regime, even though the Stokes number would depend on the Reynolds number Re (Whipple 1972), we deliberately do not use the Re dependency of the Stokes number for large Re for the sake of simplicity as it would require iterations to calculate it (Re depends on the differential velocity between gas and dust, which in turn depends on the stopping time, which is a function of Re). This amounts to limiting ourselves to the linear Stokes drag. Similarly, Okuzumi et al. (2012) neglected the high- Re domain of the Stokes regime (also known as the Newton drag regime) for simplicity. They showed that this somewhat accelerates dust growth but concluded that it has little effect of the ability of porosity to help grains to survive the radial-drift barrier. Additionally, the transition to the Newton regime would only occur in the inner disc regions for bodies larger than $\sim 100 \text{ m}$, for which self-gravity would start to be important and assist their growth. However, this is out of the scope of this paper (see Section 2.5.2).

This friction force makes the dust settle down to the mid-plane and drift towards the star. Nakagawa et al. (1986) gave the dust radial velocity as

$$v_{\text{d},R} = -\frac{\text{St}}{(1+\epsilon)^2 + \text{St}^2} \eta v_{\text{K}}, \quad (6)$$

where v_K is the Keplerian velocity and η the sub-Keplerian parameter defined as

$$\eta = - \left(\frac{H_g}{R} \right)^2 \frac{\partial \ln P_g}{\partial \ln R}, \quad (7)$$

with H_g the gas scale height and P_g the gas pressure. From equation (6), we can find again that both small and large grains, with small and large St values, drift slowly. We can also infer that dust can be slowed down by increasing the dust-to-gas ratio ϵ .

2.3 Growth model

In this study, we only consider icy dust with $\rho_s = 917 \text{ kg m}^{-3}$. Indeed, water ice can be found in large quantities exterior to the snow line (van Dishoeck et al. 2014). Furthermore, in those regions, water can condense on grains surface, change the sticking properties and promote growth over bouncing or fragmentation (Gundlach et al. 2011; Gundlach & Blum 2015). Silicate grains have a fragmentation threshold $\sim 1 \text{ m s}^{-1}$ while icy dust fragments for a relative velocity larger than several 10 m s^{-1} (Blum & Wurm 2008; Yamamoto et al. 2014). While recent laboratory experiments (Gundlach et al. 2018; Musiolik & Wurm 2019) found lower surface energies for water ice than previously used at low temperatures, thus suggesting that ice is not more resistant than silicates, they disagree with the tensile strengths measured in numerical simulations by Tatsuuma et al. (2019). Further investigation is thus needed before the issue can be settled. Thus, in this work we focus on pure growth and neglect bouncing and fragmentation, similarly to Krijt et al. (2016). This also allows to better understand the influence of porosity on these physical processes separately. The actual value of the fragmentation threshold of water ice therefore does not affect the results presented here. Bouncing and fragmentation will be taken into account in a followup paper.

We use a grain growth model with a locally mono-disperse mass distribution, in which collisions are considered to occur between identical grains. Details on the model implementation and a discussion on its assumptions can be found in Laibe et al. (2008). As fragmentation is not taken into account in this study, every collision leads to sticking. Stepinski & Valageas (1997) gave the expression of the variation of a grain’s mass with time as it doubles in a mean collision time τ_{coll} , i.e.

$$\frac{dm}{dt} \approx \frac{m}{\tau_{\text{coll}}} = 4\pi s^2 v_{\text{rel}} \rho_d = 4\pi s^2 v_{\text{rel}} \epsilon \rho_g. \quad (8)$$

Grains collide with a relative velocity v_{rel} transmitted from gas turbulent motion to the dust by aerodynamic drag. We use the Stepinski & Valageas (1997) model, in which

$$v_{\text{rel}} = \sqrt{2^{3/2} \text{Ro} \alpha} \frac{\sqrt{\text{Sc} - 1}}{\text{Sc}} c_g, \quad (9)$$

where Ro is the Rossby number for turbulent motions, taken equal to 3, and Sc the Schmidt number of the grains, whose expression is

$$\text{Sc} = (1 + \text{St}) \sqrt{1 + \frac{\Delta v^2}{v_t^2}}, \quad (10)$$

where $v_t = \sqrt{2^{1/2} \text{Ro} \alpha} c_g$ denotes the turbulent velocity. $\Delta v = v_d - v_g$ is the differential velocity between dust and gas. In our simulations, Δv appeared to be negligible compared to v_t (see also Laibe et al. 2008) and v_{rel} can be approximated as

$$v_{\text{rel}} \approx \sqrt{2^{3/2} \text{Ro} \alpha} \frac{\sqrt{\text{St}}}{1 + \text{St}} c_g. \quad (11)$$

The reader is referred to Laibe et al. (2008) for a discussion of the difference between equation (10) and the expression of Youdin & Lithwick (2007), and to Laibe (2014) for a more general discussion on various models for relative velocities.

The collisional kinetic energy E_{kin} for identical grains is then given by

$$E_{\text{kin}} = \frac{1}{2} m^* v_{\text{rel}}^2 = \frac{1}{4} m v_{\text{rel}}^2, \quad (12)$$

where the reduced mass $m^* = m/2$ for identical grains.

2.4 Model for porosity evolution during growth

We consider grains as aggregates of elementary monomers. Those monomers are compact spheres, with a density ρ_s and a radius a_0 . The volume filling factor ϕ is then used to characterise how porous the grains are. It is defined as the ratio between the volume occupied by matter V_{mat} to the total volume V of a grain:

$$\phi = \frac{V_{\text{mat}}}{V} = \frac{\rho}{\rho_s} \quad (13)$$

where ρ is the density of the grain. Compact grains have $\phi = 1$ while $\phi \sim 0$ corresponds to very fluffy aggregates.

Real porous aggregates can have arbitrary shapes and mass distributions. Parameters such as radius, cross-section or volume are therefore ill-defined. The equations presented in Sections 2.2 and 2.3 were initially derived for compact spherical grains. In this work, in order to be able to use them, as well as equation (13), we assume that a porous aggregate can be represented by an equivalent spherically-symmetric and non-fractal collection of monomers in order to describe its spatial, size and porosity evolution.

2.4.1 Collisional evolution

Small grains, with low velocities (Weidenschilling & Cuzzi 1993) meet slowly and stick, it is the “hit-and-stick” regime. Such collisions make the grains more porous, or decrease their filling factor, as their total volume grows faster than that occupied by matter (see Okuzumi et al. 2012). When grains collide with a kinetic energy larger than the rolling energy E_{roll} (see equation A4), i.e. the energy needed for one monomer to roll over 90° on the surface of another monomer (Dominik & Tielens 1997), the formed aggregate dissipates the extra energy by compressing. Thus, the grain still becomes more porous, but less than in the hit-and-stick regime (Okuzumi et al. 2012). Thanks to numerical simulations of collisions, Suyama et al. (2008) have expressed the filling factor of the grain after a collision ϕ_f in those two regimes as a function of parameters before the collision such as the kinetic energy E_{kin} or the filling factor ϕ_i of colliding grains. However, this formula is recursive and cannot be used in our simulations where a time step corresponds to any number (not necessarily an integer) of collisions. Thus, to describe the evolution of the filling factor during collisional growth ϕ_{col} , we needed to modify the Suyama et al. (2008) model to make it continuous and non-recursive. This amounts to obtaining an expression for ϕ_f only as a function of grain mass m and disc quantities. The details of our calculations and approximations are presented in Appendix A. Our resulting expressions for ϕ_{col} are:

(i) hit-and-stick

$$\phi_{\text{h\&s}} = \left(\frac{m}{m_0} \right)^{-0.58}, \quad (14)$$

where $m_0 = \frac{4}{3}\pi a_0^3 \rho_s$ is the monomer mass.

(ii) collisional compression: four cases need to be considered depending on the drag regime, Epstein or Stokes, and whether $St < 1$ or $St > 1$

$$\phi_{\text{Ep-St}<1} = \left(2^{1/5} - \beta_{\text{Ep}}\right)^{-3/8} \beta_{\text{Ep}}^{-5/8} 2^{1/8} \times \left(\frac{3}{10} \frac{(3/5)^5 2^{3/2} \text{Ro} \alpha m_0 c_g \rho_s a_0 \Omega_K}{8 \rho_g b E_{\text{roll}}}\right)^{3/8} \left(\frac{m}{m_0}\right)^{-1/8}, \quad (15)$$

$$\phi_{\text{St-St}<1} = \left(2^{1/5} - \beta_{\text{St}}\right)^{-1/3} \beta_{\text{St}}^{-2/3} \times \left(\frac{3}{10} \frac{(3/5)^5 2^{3/2} \text{Ro} \alpha m_0 c_g^2 \rho_s a_0^2 \Omega_K}{36 \mu_g b E_{\text{roll}}}\right)^{1/3}, \quad (16)$$

$$\phi_{\text{Ep-St}>1} = \phi_{\text{Ep-St}<1}(M_4) \left(\frac{m}{M_4}\right)^{-1/5}, \quad (17)$$

$$\phi_{\text{St-St}>1} = \phi_{\text{St-St}<1}(M_5) \left(\frac{m}{M_5}\right)^{-1/5}, \quad (18)$$

where M_4 and M_5 are the masses for which $St = 1$, respectively in the Epstein and Stokes regimes. They are given in equations (A16) and (A17).

2.4.2 Static compression

Kataoka et al. (2013a) have shown that very fluffy grains can be statically compressed by an applied compressive strength P . The filling factor is then linked to P as

$$\phi = \left(\frac{a_0^3}{E_{\text{roll}}} P\right)^{1/3}. \quad (19)$$

Thus, the gas drag force F_{drag} applies a compressive strength $P_{\text{drag}} = F_{\text{drag}}/(\pi s^2)$ that can compact the grain up to a value ϕ_{gas} depending on the drag regime:

$$\phi_{\text{gas}} = \begin{cases} \left(\frac{m_0 \Delta v \rho_g c_g}{\pi E_{\text{roll}} \rho_s}\right)^{1/3}, & \text{(Epstein)} \\ \left(\frac{6 a_0^2 \Delta v \mu_g}{E_{\text{roll}}}\right)^{3/8} \left(\frac{m}{m_0}\right)^{-1/8}. & \text{(Stokes)} \end{cases} \quad (20)$$

Finally, massive enough grains can be compressed by their self-gravity up to a filling factor ϕ_{grav} given by Kataoka et al. (2013b) as:

$$\phi_{\text{grav}} = \left(\frac{\mathcal{G} m_0^2}{\pi a_0 E_{\text{roll}}}\right)^{3/5} \left(\frac{m}{m_0}\right)^{2/5}. \quad (21)$$

The filling factor of dust naturally evolves as ϕ_{col} during collisions until the grain is fluffy enough to be compressed by the gas drag or its self-gravity and then its filling factor is equal to ϕ_{gas} or ϕ_{grav} respectively. Therefore, the maximum of ϕ_{col} , ϕ_{gas} and ϕ_{grav} provides the smallest possible value of the filling factor. The different regimes encountered by growing grains at fixed locations are summarised in Figure B1.

2.5 Numerical simulations

In order to model the evolution of porous dust grains in protoplanetary discs, we use two codes with different properties.

2.5.1 The PACED code

We have developed the PACED¹ code, a 1D C++ code to model the behaviour of a single grain at a time in a stationary gas disc described with power laws with a constant dust-to-gas ratio of 10^{-2} . This code contains radial drift with equation (6), the growth model described in Section 2.3 and porosity evolution with the model presented in Section 2.4.

2.5.2 3D SPH code

We also use the 3D, two-phase (gas+dust), SPH (Smoothed Particle Hydrodynamics) code described in Barrière-Fouchet et al. (2005). The code computes the dynamics of both phases, which interact via aerodynamic drag in the Epstein regime, including the back-reaction of dust on gas. (In contrast to PACED, this code does not use equation (6) but calculates the forces on each SPH particle and their ensuing motion.) It reproduces the properties of turbulence (Arena & Gonzalez 2013). Grain growth was implemented in Laibe et al. (2008) and fragmentation in Gonzalez et al. (2015a). Self-gravity is not included. Detailed discussions of the code properties can be found in Fouchet et al. (2007) and Gonzalez et al. (2017a). In this work, we have added the implementation of the Stokes drag regime to consider the evolution of the largest solids. We have also included our model of porosity evolution.

We start the simulations presented here with 200,000 SPH gas particles arranged to reproduce the power laws presented in Section 2.1 and let the disc relax for 24 orbits at $R = 100$ AU for the CTTS disc and $R = 40$ AU in the Flat disc. Then, the same number of SPH dust particles is injected at the same locations and velocities as the gas particles, to recreate an initial dust-to-gas ratio $\epsilon = 10^{-2}$. Both sets of particles are then evolved together. Previous work with the same code (e.g. Barrière-Fouchet et al. 2005; Fouchet et al. 2007; Pignatale et al. 2019) has shown that convergence is reached at lower particle numbers. We also verify that the resolution criterion from Laibe & Price (2012) is met. Each SPH dust particle represents a collection of identical physical dust grains (locally mono-disperse assumption, see Section 2.3) and carries intrinsic dust properties such as mass, filling factor and thus, size, that are described according to the models presented in Sections 2.3 and 2.4. In particular, we chose a uniform initial size $s_0 = 10 \mu\text{m}$ for all grains to shorten the computation times. Indeed, we have previously shown that very small grains grow fast and quickly forget their initial size (Laibe et al. 2008). Their corresponding initial filling factor and mass, which depend on their location, are pre-calculated with the PACED code by evolving compact monomers of size a_0 without radial drift. The simulations are stopped when the largest grains reach kilometre sizes, for which self-gravity becomes important, because both our growth model and our SPH code do not take it into account. Obtaining estimates of the fraction of dust that would turn into planetesimals or of properties of the resulting planetesimal population is therefore not feasible in the framework of our study.

¹ for Porous And Compact dust Evolution in Discs

Table 2. Comparison between our PACED and 3D SPH codes.

Characteristics	PACED	3D SPH
dynamics	X	X
growth	X	X
porosity	X	X
turbulence		X
disc evolution		X
collective effects		X

2.5.3 Comparison

As summarised in Table 2 and contrary to the PACED code, our 3D SPH code models the evolution of the gas disc and takes into account the collective effects. Indeed, dust drift can change the local dust-to-gas ratio which has an impact on dust growth and dynamics, while it is taken constant in the PACED code. However, the 3D SPH code requires long calculation times and is not practical to study a large variety of cases. Thus, we use the PACED code to test our model and estimate the dust behaviour on larger time scales. Moreover, in the PACED code, disc quantities such as gas density or differential velocity between gas and dust are obtained from analytical prescriptions while in the 3D SPH code, they are computed self-consistently (Barrière-Fouchet et al. 2005).

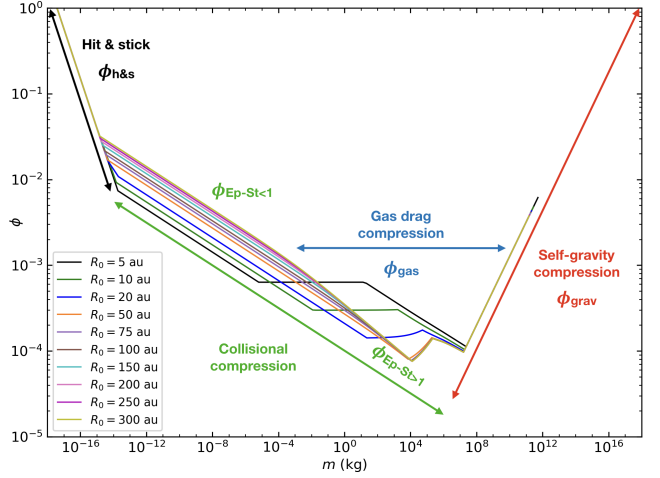
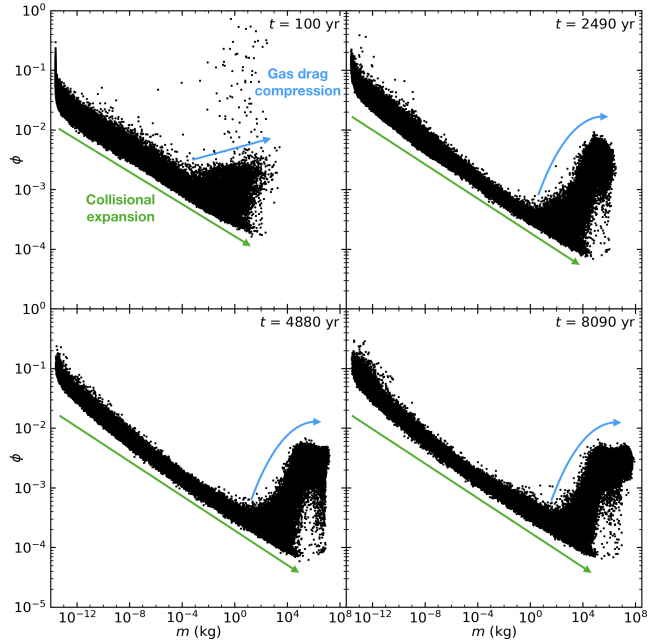
3 RESULTS

In Sections 3.1 and 3.2, we present how porosity evolves during dust growth and how it impacts growth and dynamics in the CTTS disc with monomer size $a_0 = 0.1 \mu\text{m}$. In Section 3.3, we show the influence of the monomer size a_0 on porosity and thus, on growth in the Flat disc.

3.1 Evolution of the filling factor

Figure 1 shows the evolution of the filling factor of grains of different initial positions as a function of their mass as they grow and drift radially, computed with the PACED code. The curves have similar shapes to those found by Kataoka et al. (2013b) for grains at fixed distances from the star (see also our model at fixed distances in Fig. B1 for comparison): ϕ first decreases due to collisions, then increases again with gas drag compression before self-gravity is strong enough to compact the grains further. However, inwards drifting grains experience different disc conditions, and in particular larger gas densities, than static ones and are all the more compacted by gas drag as they are close to the star. Their minimum filling factor, $\sim 10^4$, is somewhat larger and it is reached for smaller masses.

The time evolution of the grain filling factor computed with the 3D SPH code is displayed in Fig. 2. Initially, $10\text{-}\mu\text{m}$ sized grains have a filling factor of $\sim 10^{-1} - 10^{-2}$, according to their initial location in the disc. As dust grows, representative dots move to the right. At first, grains are in the collisional compression regime. This regime tends to make grains more and more porous until they are fluffy enough to be compressed by gas drag. Note that the gas drag compression regime has a different shape than that computed with the PACED code (Fig. 1), illustrating the differences between


Figure 1. Filling factor as a function of mass in the CTTS disc for drifting grains of different initial positions R_0 with the PACED code. Arrows show the different regimes encountered by the grains.

Figure 2. Time evolution of the filling factor as a function of mass for grains in the CTTS disc with the 3D SPH code. Representative dots move to the right as grains grow. The filling factor decreases thanks to the collisional expansion regime (green arrow) then increases because of the compression due to the gas drag (blue arrow).

both codes listed in Section 2.5.3. In the top left panel, some dots move upwards with a quasi constant mass. Those dots correspond to grains that are quickly compacted by gas drag as they are accreted into the central star. The minimum value of ϕ , also $\sim 10^4$, is consistent with the numerical simulations of collisions of Kempf et al. (1999).

Figure 3 shows the distribution of the filling factor through the disc. A vertical sorting of the filling factor occurs: more compact grains are located along the disc surface while grains are fluffier and fluffier as they are closer to the mid-plane. Indeed, grains grow

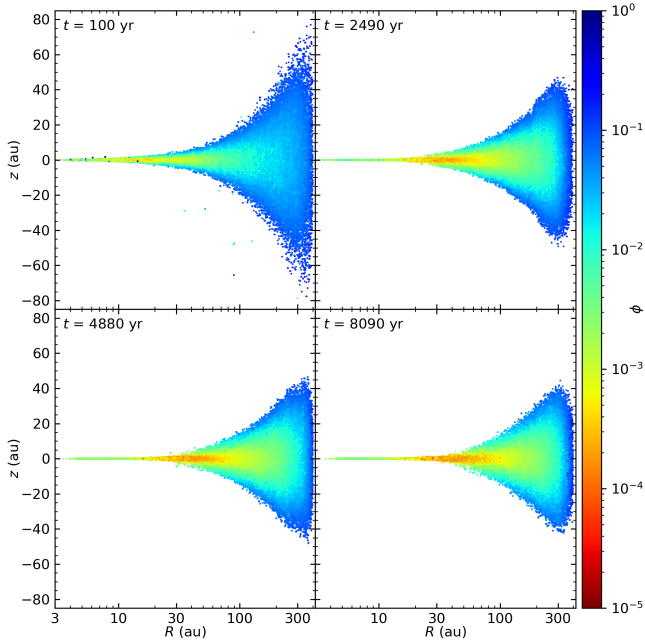


Figure 3. Time evolution of the dust distribution in the CTTS disc with the 3D SPH code. The colour bar represents the filling factor.

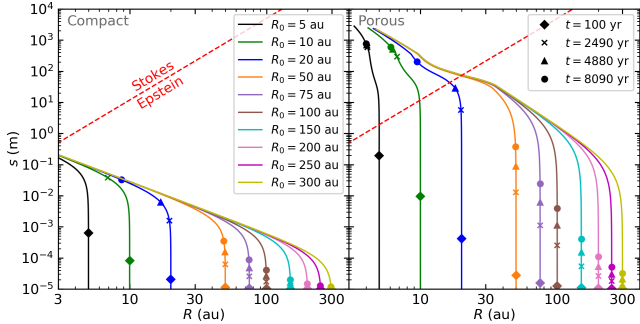


Figure 4. Grain size as a function of the distance from the star in the CTTS disc for different initial positions R_0 with the PACED code, for compact (left) and porous (right) dust. The red dashed line marks the limit between the Epstein and Stokes regimes. The symbols show the value of the size at the same time steps as in Fig. 5.

more rapidly in denser regions (equation 8) and thus reach lower filling factors in the collisional regime. The same effect is seen in the radial direction. However, grains in the disc innermost regions are compacted because it is there that gas drag compression is mostly effective, where the gas is dense enough.

3.2 Influence on grain size and dynamics

Figure 4 compares the radial evolution of the size of compact and porous grains, computed with the PACED code. Compact and porous grains both have a qualitatively similar behaviour: they first grow at a quasi-constant distance from the star until they approach an optimal size $s_{St=1}$, for which $St = 1$ and radial drift is the fastest. They then drift rapidly inwards while continuing to grow before slowing down close to the star, where they finally keep growing while drifting very little. These three stages were described and ex-

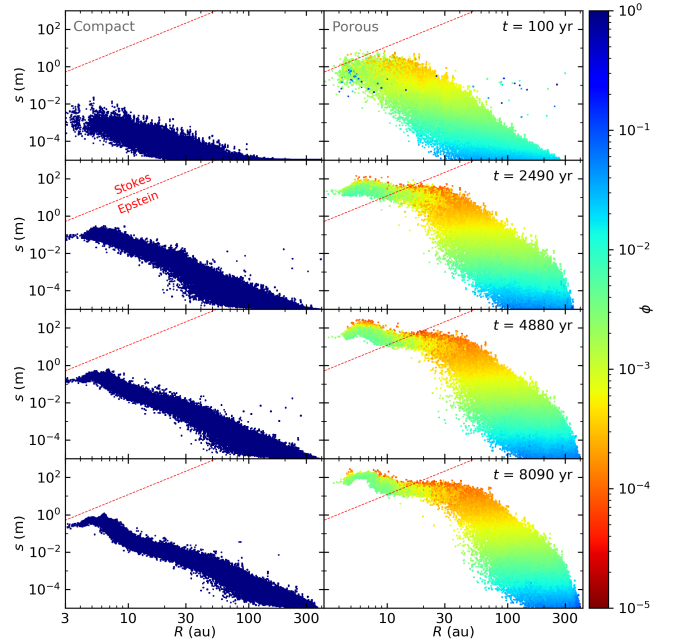


Figure 5. Radial grain size distribution in the CTTS disc obtained with the 3D SPH code. Porous grains (right) can reach larger sizes than compact dust (left). The colour bar represents the filling factor. The red dashed line in the top left corner separates the Epstein (below the line) and Stokes (above the line) drag regimes. Four snapshots at 100, 2490, 4880 and 8090 yr are shown, from top to bottom.

plained by Laibe et al. (2008). During the second stage, compact grains gain 1 to 3 orders of magnitude in size before reaching the disc inner regions, depending on their initial location, while porous grains can gain up to 4. Indeed, since $s_{St=1}$ is larger for porous grains (see Fig. 9), they have a larger cross section and grow more rapidly (equation 8): the slope in Fig. 4 is steepest. These results are in agreement with those found by Okuzumi et al. (2012).

The time evolution of the radial grain size distribution of compact and porous grains computed with the 3D SPH code is plotted on Fig. 5. Here as well, porous grains experience a quicker growth than compact grains. In 8090 yr, in the inner disc, the largest porous grains have planetesimal sizes and are in the Stokes drag regime while compact grains hardly reach one meter and stay in the Epstein regime. Furthermore, growth is very slow for compact dust beyond 100 au and grains cannot grow beyond 100 μm . On the contrary, porous dust can reach centimetre sizes up to 300 au and metre sizes interior to 100 au. The right column of Fig. 5 shows that small grains are only slightly porous. As they grow, they become fluffier and fluffier and are compressed in the inner regions of the disc as seen in Fig. 3 as well.

Fig. 6 shows the time evolution of the dust spatial distribution of compact and porous grains computed with the 3D SPH code. In both cases, dust is vertically size-sorted. Larger solids can be found close to the mid-plane while small grains are distributed over a larger scale height. In the porous case, the mid-plane is filled with ~ 100 m solids from the inner edge out to ~ 50 au. Two differences on dynamics can be also spotted out. After 8090 yr, the disc made of compact dust is approximately 20 au less radially extended than with porous grains. Moreover, this disc is also more settled compared to the one with fluffy dust. Indeed, porous grains can stay

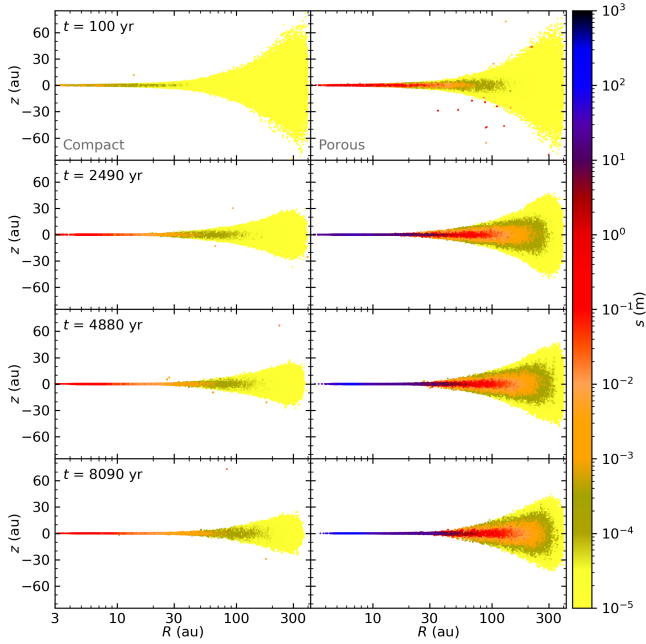


Figure 6. Time evolution of the dust distribution in the CTTS disc obtained with the 3D SPH code. The colour bar represents the grain size. Porous grains (right) are less settled than compact dust (left). Four snapshots at 100, 2490, 4880 and 8090 yr are shown, from top to bottom.

coupled with the gas phase ($St \ll 1$) at larger sizes than compact grains, they settle down and drift inward slightly less rapidly.

3.3 Influence of monomer size

Figure 7 compares the time evolution of the filling factor during growth for grains made of monomers of different sizes $a_0 = 0.1$ and $1 \mu\text{m}$ in the Flat disc. The behaviours are similar to the CTTS disc (Fig. 2). Initially, grains are in the collisional expansion regime then are compacted because of the gas drag. Grains reach similar masses in both cases, large enough to be compressed by their self-gravity as indicated by the red arrow. All these regimes depend on the monomer size and the filling factor increases when a_0 increases, see equations (14)–(21). Thus, $10\text{-}\mu\text{m}$ sized grains composed of $1\text{-}\mu\text{m}$ monomers are more massive than those made of $0.1\text{-}\mu\text{m}$ monomers. One can observe that gas drag compression is almost as efficient in both cases, i.e. it compresses grains to similar filling factors. However, since grains made of large monomers are already more compact, their change in filling factor is smaller during that phase. In the same way, self-gravity starts to compact the dust at a larger mass.

The radial size distribution is compared in Fig. 8. At first, the difference in filling factor does not affect much the radial extension of the disc, i.e. the radial drift is not influenced by the monomer size. The main impact of the porosity change is on growth. Since grains composed of large monomers are less porous, they grow less efficiently and produce less large grains. Dust made of $0.1\text{-}\mu\text{m}$ monomers can produce planetesimals in the innermost 100 au of the disc while it is only the case over a few au with $1\text{-}\mu\text{m}$ monomers.

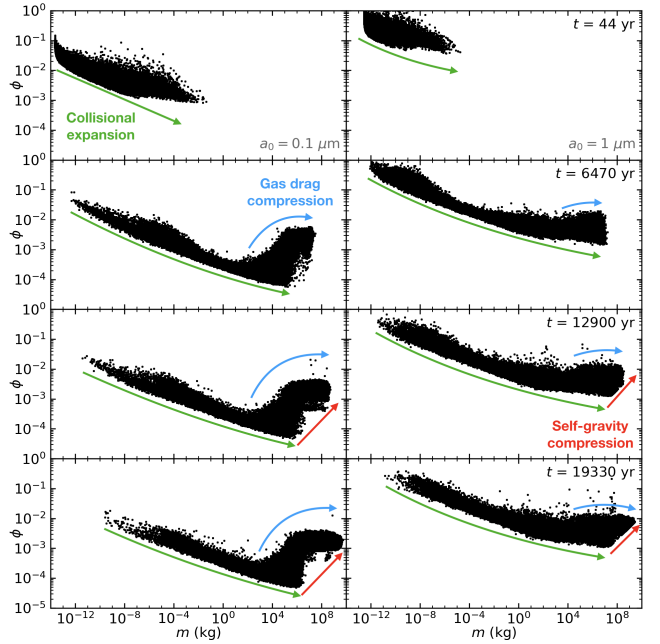


Figure 7. Time evolution of the filling factor as a function of mass for grains in the Flat disc obtained with the 3D SPH code. Porous grains that are made of $0.1 \mu\text{m}$ monomers (left) can become more porous than grains formed with $1 \mu\text{m}$ monomers (right). However, the filling factor has a similar behaviour in both cases: it decreases thanks to the collisional expansion regime (green arrow) then increases because of the compression due to the gas drag (blue arrow) and finally, grains reach the self-gravity compression regime (red arrow). Four snapshots at 44, 6470, 12900 and 19330 yr are shown, from top to bottom.

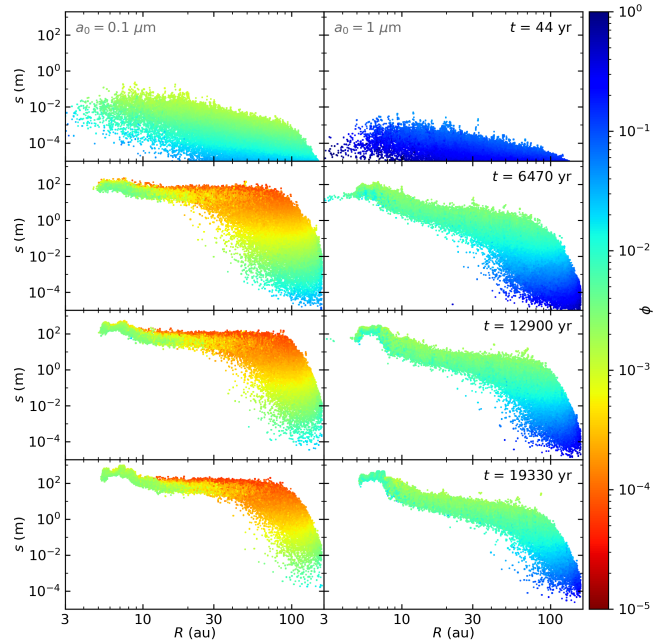


Figure 8. Time evolution of the radial grain size distribution in the Flat disc obtained with the 3D SPH code. Aggregates made of $0.1\text{-}\mu\text{m}$ monomers (left) can reach larger sizes all over the disc than dust made of $1\text{-}\mu\text{m}$ monomers (right). The colour bar represents the filling factor. Four snapshots at 44, 6470, 12900 and 19330 yr are shown, from top to bottom.

4 DISCUSSION

4.1 Porosity in the Solar System

Okuzumi et al. (2012) studied the possibility of forming planetesimals from direct growth of porous dust. This idea was then completed by Kataoka et al. (2013b) who added the compression due to gas drag and self-gravity of massive solids. They have thus determined the evolution of the filling factor during growth but without drift and collective effects in a Minimum Mass Solar Nebula (MMSN) disc. With our continuous model, the values we obtain are generally in a good agreement with those from Kataoka et al. (2013b). The minimum value reached by the filling factor, $\sim 10^{-4}$, is however slightly larger than that of Kataoka et al. (2013b) because our grains drift to regions where the gas density is larger, and hence gas drag compression stronger.

The Solar System still contains porous bodies today. Evidence has been found for low densities in asteroids, such as 253 Mathilde (Housen et al. 1999; Veverka et al. 1999), or meteorites (e.g. Brown et al. 2002). This may even be a more widespread property, with the recent suggestion that the first known interstellar object to visit our system, 1I/Oumuamua, is a fractal dust aggregate with an ultra-low density of $10^{-2} \text{ kg m}^{-3}$ (Flekkøy et al. 2019). Spatial exploration and measurements on comets have shown that these objects made of ice and silicates are also porous. Their average density falls between 400 and 600 kg m^{-3} (Blum et al. 2006; A’Hearn 2011). As an example, Sierks et al. (2015) determined that the density of comet 67P/Churyumov-Gerasimenko is of the order of 470 kg m^{-3} . The *Rosetta* probe orbiting comet 67P and its lander *Philae* have provided a wealth of data on this body. In particular, they have shown that its surface is covered with solids whose size varies from tens of micrometers to tens of meters (Blum et al. 2017). Among them, millimeter-sized grains with a density $< 1 \text{ kg m}^{-3}$ and a filling factor $\phi \sim 10^{-3}$ were found with the GIADA instrument (Fulle et al. 2015). As can be seen on Fig. 5, our results show that grains with similar sizes and filling factors are present over large regions in the disc. While such low filling factors can seem surprising at first, they are compatible with the measurements made on comet 67P.

4.2 The Stokes regime, a key point

One of the main theoretical problems for dust evolution is the radial-drift barrier, i.e. the rapid inwards drift of grains with $St = 1$ leading to dust accretion onto the star. A solution to this problem is either to stop the grains from drifting or for them to grow from $St \ll 1$ to $St \gg 1$ (for which the drift is slow) in a time shorter than the drift timescale.

Moreover, Laibe et al. (2012) have shown that if dust reaches $St > 1$ in the Stokes drag regime, it remains in the disc if $q \leq 2/3$. Discs satisfying this condition represent 90% of discs observed by Andrews & Williams (2005, 2007). The Stokes regime has two advantages: the Stokes number increases as grains get closer to the star (while it decreases in the Epstein regime) and varies as s^2 (while as s in the Epstein regime), see equation (5)². Thus, in the Stokes drag regime, dust can reach large Stokes numbers more easily. Physically, it means that the grain is more efficiently slowed down by the stronger gas drag in the inner parts of the disc. Consequently, reaching the Stokes drag regime with $St \sim 1$ is a key point

² For a power-law disc, $St \propto s R^p$ in the Epstein regime and $St \propto s^2 R^{(q-3)/2}$ in the Stokes regime.

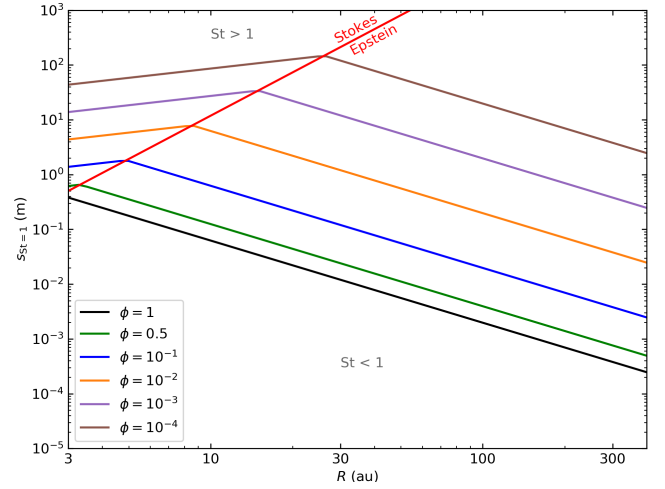


Figure 9. Optimal size, i.e. size for which $St = 1$, as a function of the distance from the star in the CTTS disc for different filling factor values. For a given filling factor, below the line, grains have $St < 1$ and above it $St > 1$. The red line represents the limit between the Epstein and Stokes regimes for $s = 9\lambda/4$. Above this line, grains are in the Stokes regime and $St \propto s^2$ while below, they are in the Epstein regime and $St \propto s$.

for grains to remain in most discs and thus survive the radial-drift barrier.

In order to understand the influence of porosity on the Stokes number and the drag regime, one needs to compare two characteristic sizes:

- the optimal size, $s_{St=1}$, for which the grain Stokes number reaches unity, i.e. the size corresponding to the fastest drift;
- $9\lambda/4$, the transition size between the Epstein and Stokes drag regimes.

In a power-law disc, the optimal size $s_{St=1} \propto \phi^{-1} R^{-p}$ in the Epstein regime and $s_{St=1} \propto \phi^{-1/2} R^{(3-q)/4}$ in the Stokes regime. $9\lambda/4$ does not depend on the filling factor and varies as $R^{p+(3-q)/2}$. If $s_{St=1} < 9\lambda/4$ (resp. $s_{St=1} > 9\lambda/4$), grains reach the maximal drift velocity in the Epstein (resp. Stokes) regime.

Figure 9 shows the optimal size for different filling factors and the transition between both drag regimes. For compact grains, the transition between the Epstein and Stokes regimes occurs necessarily with $St > 1$. It means that compact grains experience a maximal inwards drift (and accretion onto the star) without the chance to transition to the Stokes regime. On the contrary, for grains with a filling factor lower than 0.5, there exists a region in the inner disc where porous grains are in the Stokes drag regime with $St \leq 1$, which is more and more extended as grains become fluffier and fluffier. Thus, the Stokes number of those grains can increase rapidly during their growth, allowing them to decouple from the gas and survive the radial-drift barrier.

4.3 Porosity and growth

As discussed previously, porosity can have an impact on dust spatial evolution and growth. According to Figs. 4 and 5, compact and porous grains have a qualitatively similar growth behaviour in three stages. The optimal size for compact grains is about 0.1 mm. Since the optimal size depends on the grain filling factor, porous grains can reach larger sizes before starting to drift rapidly. For instance, porous grains with $\phi = 10^{-3}$, order of magnitude of the average

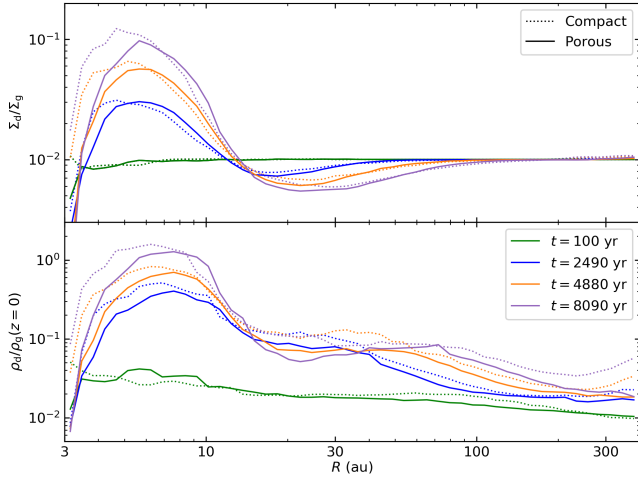


Figure 10. Azimuthally-averaged radial profiles of the dust-to-gas ratio: vertically integrated (top) and in the mid-plane (bottom) for different time steps obtained with a 3D SPH simulation of the CTTS disc. Porous grains are represented by solid lines and compact grains by dotted lines. In the PACED code, the dust-to-gas ratio has a constant value of 10^{-2} .

filling factor over the disc (Fig. 5), have an optimal size 10^3 times larger than for compact grains. Thus, they can grow up to ~ 10 cm before drifting significantly. This average ratio of 10^3 for porous grains sizes can be seen in Figs. 4 and 5. Generally, porous dust is characterised by a more efficient growth during the three steps described previously as their collision cross-section is larger than for compact grains. Consequently, porosity helps grains to reach larger sizes and transition to the Stokes drag regime in the inner disc, as seen in Figs. 4 and 5. We discussed in Section 4.2 on how the Stokes drag regime is important for the dust survival in the disc.

Porosity also allows to form 100 m – 1 km planetesimals in the mid-plane in the innermost 100 au, as shown by Figs. 4 and 6, in less than 10^4 yr. Even if our disc model is different from the one Krijt et al. (2016) use, we find drift and growth timescales for both compact and porous grains similar to theirs. Those planetesimals are thought to be building blocks to form giant planet cores and our results can be used as a starting point for simulations of giant planet formation (Kobayashi et al. 2016; Kobayashi & Tanaka 2018).

4.4 On drift and the importance of collective effects

We can spot a different behaviour for compact dust in the very inner disc. With the PACED code, compact dust is accreted onto the star without growing larger than the decimetre (Fig. 4), while we find in 3D SPH simulations that compact solids can remain in the very inner disc where they can reach metre sizes (Fig. 5). This phenomenon can be explained by the different calculation (and influence) of the local dust-to-gas ratio ϵ in our two codes. Indeed, Nakagawa et al. (1986) have shown (via equation (6)) that dust drift is slowed down when the local dust-to-gas ratio increases thanks to dust collective effects. Moreover, the PACED code uses a constant ϵ of 10^{-2} while in the 3D SPH code, this quantity is directly calculated using the local dust and gas densities and so may vary. Figure 10 reports the value of the dust-to-gas ratio at several times of the simulation with our 3D SPH code. Initially, $\epsilon = 10^{-2}$ in the whole disc as in the PACED code but as grains grow, they drift inwards and the dust-to-gas ratio increases in the innermost few au

where its vertically integrated value can reach 10^{-1} . In the mid-plane, it can even exceed unity thanks to vertical settling. Thus, the drift is slowed down and growth accelerated as the dust phase is denser. Those two effects help compact grains to reach meter sizes at the edge of the disc. However, they are not strong enough to allow them to reach the Stokes regime.

Such an increase in the dust-to-gas ratio in the inner disc was not seen for compact grains by Birnstiel et al. (2010), Okuzumi et al. (2012), or Krijt et al. (2016), whose framework and assumptions are very different from ours. These previous studies are all one-dimensional and compute the vertically-averaged dust evolution in the radial direction while keeping the gas distribution fixed (amounting to neglecting the back-reaction of dust on gas) and assuming vertical hydrostatic equilibrium for the gas and a prescription for the dust vertical scale-height as a function of turbulence. Okuzumi et al. (2012) further assess the impact of back-reaction on the velocities of gas and dust and on collision velocities and find it to be negligible. However, it is not a full implementation of back-reaction as the background gas structure is still kept constant. For compact dust, all these studies found that grains grow until they reach $St = 1$ then drift inwards, producing a drift-limited size distribution and a flat dust-to-gas ratio profile. On the contrary, our simulations are three-dimensional and compute the self-consistent evolution of both gas and dust, including back-reaction of dust on gas. It has been shown that back-reaction, assisted by an increase of dust density close to the mid-plane due to vertical settling, is able to slow down the dust radial drift enough to allow grains to grow to sizes for which $St > 1$, slow down their drift further, and pile up (e.g. Laibe et al. 2008; Gonzalez et al. 2015b, 2017a), something models neglecting back-reaction are unable to capture. The importance of back-reaction has further been shown by several authors (e.g. Kanagawa et al. 2017; Dipierro & Laibe 2017; Dipierro et al. 2018). The reader is referred to Gonzalez et al. (2017a) for a comparison of dust-to-gas ratio profiles with and without back-reaction in the case when dust fragmentation is included.

For porous dust, Okuzumi et al. (2012) and Krijt et al. (2016) found that grains grow rapidly, overcome the radial-drift barrier, then pile up, leading to an increase of the dust-to-gas ratio in the inner disc. This is exactly what we find in this study, see Section 3.2 and Fig. 10. However, where Okuzumi et al. (2012) saw an increase of their one-dimensional ϵ of a factor of several, our azimuthally-averaged, vertically-integrated ϵ is enhanced by one order of magnitude. Porous grains, similarly to compact grains, experience collective effects, which play an important role in setting their spatial distribution. Additionally, even though porosity can slightly slow down vertical settling and radial drift, its main effect remains a strong acceleration of growth (Section 3.2), which causes the transition to the Stokes drag regime. As a result, porous grains decouple from the gas and pile-up sooner in their evolution, therefore at larger distances from the star, than compact grains. This is reflected in the locations of the dust-to-gas ratio maxima in Fig. 10. The combination of collective effects and of the Stokes regime also results in a larger dust-to-gas ratio than when dust back-reaction is not included.

5 CONCLUSION

The growth from sub- μ m monomers to planetesimals is hampered by several barriers such as the radial-drift barrier. The dust needs to decouple from the gas in order to remain in the disc. In this work, we investigate how porosity can act on both grain growth and drift

to overcome this barrier. It amounts to considering simultaneously, and thus link, the small (collisions) and large (disc) scales. To do so, we have developed a model of evolution of the filling factor depending on grain characteristics (bulk density, rolling energy, mass) and disc quantities (gas density, sound speed or temperature). Our model can be used for codes in which the disc evolution time step is different from that of individual collisions. We demonstrate that grains can remain in the disc in most cases if they grow enough to transition to the Stokes drag regime. Indeed, in this regime, dust can reach large Stokes numbers and decouple from the gas more easily. We have shown that compact grains do not grow quickly enough and stay in the Epstein regime. However, collective effects can slow them down enough for them to remain in the very inner regions of the CTTS disc. We find that the growth is accelerated for porous grains, allowing them to transition to the Stokes regime close to the star and survive the radial-drift barrier, both in the CTTS and Flat discs. Furthermore, our study has shown that porous millimetre grains have an average filling factor of about 10^{-3} , in good agreement with measurements made on comet 67P/Churyumov-Gerasimenko (Fulle et al. 2015). Finally, we find that small planetesimals can be formed by direct coagulation of porous dust in the innermost 100 au. This result provides a link with the formation of giant planet cores from planetesimals.

ACKNOWLEDGEMENTS

We thank the anonymous referee for their careful reading and assessment of our work, which helped to improve this paper. The authors acknowledge funding from ANR (Agence Nationale de la Recherche) of France under contract number ANR-16-CE31-0013 (Planet-Forming-Disks). This research was partially supported by the Programme National de Physique Stellaire and the Programme National de Planétologie of CNRS/INSU, France. AJLG and JFG thank the LABEX Lyon Institute of Origins (ANR-10-LABX-0066) of the Université de Lyon for its financial support within the programme ‘Investissements d’Avenir’ (ANR-11-IDEX-0007) of the French government operated by the ANR. Simulations were run at the Common Computing Facility (CCF) of LABEX LIO. All figures were made with the Python library `matplotlib` (Hunter 2007).

REFERENCES

- A’Hearn M. F., 2011, *ARA&A*, 49, 281
- Adachi I., Hayashi C., Nakazawa K., 1976, *Progress of Theoretical Physics*, 56, 1756
- Andrews S. M., Williams J. P., 2005, *ApJ*, 631, 1134
- Andrews S. M., Williams J. P., 2007, *ApJ*, 671, 1800
- Arena S. E., Gonzalez J.-F., 2013, *MNRAS*, 433, 98
- Ayliffe B. A., Laibe G., Price D. J., Bate M. R., 2012, *MNRAS*, 423, 1450
- Barge P., Sommeria J., 1995, *A&A*, 295, L1
- Barrière-Fouchet L., Gonzalez J.-F., Murray J. R., Humble R. J., Maddison S. T., 2005, *A&A*, 443, 185
- Birnstiel T., Dullemond C. P., Brauer F., 2010, *A&A*, 513, A79
- Blum J., 2004, in Witt A. N., Clayton G. C., Draine B. T., eds, *Astronomical Society of the Pacific Conference Series Vol. 309, Astrophysics of Dust*. p. 369
- Blum J., Wurm G., 2000, *Icarus*, 143, 138
- Blum J., Wurm G., 2008, *ARA&A*, 46, 21
- Blum J., Schräpler R., Davidsson B. J. R., Trigo-Rodríguez J. M., 2006, *ApJ*, 652, 1768
- Blum J., et al., 2017, *MNRAS*, 469, S755
- Brauer F., Henning T., Dullemond C. P., 2008, *A&A*, 487, L1
- Brown P. G., Revelle D. O., Tagliaferri E., Hildebrand A. R., 2002, *Meteoritics and Planetary Science*, 37, 661
- Chapman S., Cowling T. G., 1970, *The mathematical theory of non-uniform gases. an account of the kinetic theory of viscosity, thermal conduction and diffusion in gases*. Cambridge University Press
- Chokshi A., Tielens A. G. G. M., Hollenbach D., 1993, *ApJ*, 407, 806
- Dipierro G., Laibe G., 2017, *MNRAS*, 469, 1932
- Dipierro G., Laibe G., Alexander R., Hutchison M., 2018, *MNRAS*, 479, 4187
- Dominik C., Tielens A. G. G. M., 1997, *ApJ*, 480, 647
- Drążkowska J., Alibert Y., 2017, *A&A*, 608, A92
- Drążkowska J., Windmark F., Dullemond C. P., 2014, *A&A*, 567, A38
- Epstein P. S., 1924, *Physical Review*, 23, 710
- Flekkøy E. G., Luu J., Toussaint R., 2019, *ApJ*, 885, L41
- Fouchet L., Maddison S. T., Gonzalez J.-F., Murray J. R., 2007, *A&A*, 474, 1037
- Fouchet L., Gonzalez J. F., Maddison S. T., 2010, *A&A*, 518, A16
- Fulle M., et al., 2015, *ApJ*, 802, L12
- Garcia A., 2018, Phd thesis, Université de Lyon, <https://tel.archives-ouvertes.fr/tel-01977317/document>
- Gonzalez J.-F., Laibe G., Maddison S. T., Pinte C., Ménard F., 2015a, *Planet. Space Sci.*, 116, 48
- Gonzalez J. F., Laibe G., Maddison S. T., Pinte C., Ménard F., 2015b, *MNRAS*, 454, L36
- Gonzalez J.-F., Laibe G., Maddison S. T., 2017a, *MNRAS*, 467, 1984
- Gonzalez J. F., Laibe G., Maddison S. T., 2017b, *MNRAS*, 472, 1162
- Gundlach B., Blum J., 2015, *ApJ*, 798, 34
- Gundlach B., Kilias S., Beitz E., Blum J., 2011, *Icarus*, 214, 717
- Gundlach B., et al., 2018, *MNRAS*, 479, 1273
- Haghighipour N., 2005, *MNRAS*, 362, 1015
- Housen K. R., Holsapple K. A., Voss M. E., 1999, *Nature*, 402, 155
- Hunter J. D., 2007, *Computing in Science & Engineering*, 9, 90
- Kanagawa K. D., Ueda T., Muto T., Okuzumi S., 2017, *The Astrophysical Journal*, 844, 142
- Kataoka A., Tanaka H., Okuzumi S., Wada K., 2013a, *A&A*, 554, A4
- Kataoka A., Tanaka H., Okuzumi S., Wada K., 2013b, *A&A*, 557, L4
- Kempf S., Pfalzner S., Henning T. K., 1999, *Icarus*, 141, 388
- Kobayashi H., Tanaka H., 2018, *ApJ*, 862, 127
- Kobayashi H., Tanaka H., Okuzumi S., 2016, *ApJ*, 817, 105
- Kretke K. A., Lin D. N. C., 2007, *ApJ*, 664, L55
- Krijt S., Ormel C. W., Dominik C., Tielens A. G. G. M., 2016, *A&A*, 586, A20
- Laibe G., 2014, *MNRAS*, 437, 3037
- Laibe G., Price D. J., 2012, *MNRAS*, 420, 2345
- Laibe G., Gonzalez J.-F., Fouchet L., Maddison S. T., 2008, *A&A*, 487, 265
- Laibe G., Gonzalez J.-F., Maddison S. T., 2012, *A&A*, 537, A61
- Meheut H., Meliani Z., Varniere P., Benz W., 2012, *A&A*, 545, A134
- Musiolik G., Wurm G., 2019, *ApJ*, 873, 58
- Nakagawa Y., Sekiya M., Hayashi C., 1986, *Icarus*, 67, 375
- Okuzumi S., Tanaka H., Sakagami M.-a., 2009, *ApJ*, 707, 1247
- Okuzumi S., Tanaka H., Kobayashi H., Wada K., 2012, *ApJ*, 752, 106
- Ormel C. W., Spaans M., Tielens A. G. G. M., 2007, *A&A*, 461, 215
- Paardekooper S.-J., Mellema G., 2004, *A&A*, 425, L9
- Pignatale F. C., Gonzalez J. F., Bourdon B., Fitoussi C., 2019, *MNRAS*, 490, 4428
- Pinilla P., Benisty M., Birnstiel T., 2012, *A&A*, 545, A81
- Safronov V. S., 1972, *Evolution of the protoplanetary cloud and formation of the earth and planets.. Keter Publishing House*
- Seizinger A., Speith R., Kley W., 2012, *A&A*, 541, A59
- Shakura N. I., Sunyaev R. A., 1973, *A&A*, 24, 337
- Sierks H., et al., 2015, *Science*, 347, aaa1044
- Stepinski T. F., Valageas P., 1996, *A&A*, 309, 301
- Stepinski T. F., Valageas P., 1997, *A&A*, 319, 1007
- Suyama T., Wada K., Tanaka H., 2008, *ApJ*, 684, 1310
- Suyama T., Wada K., Tanaka H., Okuzumi S., 2012, *ApJ*, 753, 115
- Tatsumi M., Kataoka A., Tanaka H., 2019, *ApJ*, 874, 159
- Veverka J., et al., 1999, *Icarus*, 140, 3

- Wada K., Tanaka H., Suyama T., Kimura H., Yamamoto T., 2007, *ApJ*, **661**, 320
- Wada K., Tanaka H., Suyama T., Kimura H., Yamamoto T., 2008, *ApJ*, **677**, 1296
- Wada K., Tanaka H., Suyama T., Kimura H., Yamamoto T., 2009, *ApJ*, **702**, 1490
- Weidenschilling S. J., 1977, *MNRAS*, **180**, 57
- Weidenschilling S. J., Cuzzi J. N., 1993, in Levy E. H., Lunine J. I., eds, *Protostars and Planets III*. University of Arizona Press, Tucson, Arizona, p. 1031
- Whipple F. L., 1972, in Elvius A., ed., *From Plasma to Planet*. Wiley Interscience Division, New York, p. 211
- Yamamoto T., Kadono T., Wada K., 2014, *ApJ*, **783**, L36
- Youdin A. N., Lithwick Y., 2007, *Icarus*, **192**, 588
- Zhu Z., Nelson R. P., Dong R., Espaillat C., Hartmann L., 2012, *ApJ*, **755**, 6
- Zhu Z., Stone J. M., Rafikov R. R., Bai X.-n., 2014, *ApJ*, **785**, 122
- van Dishoeck E. F., Bergin E. A., Lis D. C., Lunine J. I., 2014, *Protostars and Planets VI*, pp 835–858

APPENDIX A: MODEL OF POROSITY EVOLUTION DURING COLLISIONS

Suyama et al. (2008) have found that the filling factor after collision ϕ_f is related to the filling factor ϕ_i and some other quantities such as the kinetic energy E_{kin} before collision by

$$\phi_f = \begin{cases} 2\phi_i \left[2.99^{5/6} + (2 - 2.99^{5/6}) \frac{E_{\text{kin}}}{3bE_{\text{roll}}} \right]^{-6/5}, & \text{for } E_{\text{kin}} \leq 3bE_{\text{roll}} \text{ (hit and stick regime)} \\ \frac{2m_i}{\rho_s} \left[\frac{(3/5)^5 (E_{\text{kin}} - 3bE_{\text{roll}})}{N_{\text{tot}}^5 b E_{\text{roll}} V_0^{10/3}} + (2V_i^{5/6})^{-4} \right]^{3/10}, & \text{for } E_{\text{kin}} \geq 3bE_{\text{roll}} \text{ (internal restructuring regime)} \end{cases} \quad (\text{A1})$$

where m_i is the mass of colliding grains and V_i their volume. N_{tot} is the total number of monomers involved in the collision, V_0 is the volume of a monomer, defined as a compact sphere of radius a_0 and b is a numerical factor taken as 0.15 (Okuzumi et al. 2012).

The rolling energy is given by Dominik & Tielens (1997) as

$$E_{\text{roll}} = 6\pi^2 \gamma a_0 \xi_{\text{crit}}, \quad (\text{A2})$$

where γ is the surface energy of the material. They find that ξ_{crit} , the critical rolling distance of one monomer on another for energy dissipation, is of the same order as the critical distance for monomer separation, given by Chokshi et al. (1993) as

$$\delta_c = \left(\frac{27\pi^2 \gamma^2 a_0}{2\mathcal{E}} \right)^{1/3}, \quad (\text{A3})$$

where \mathcal{E} is the Young modulus of the material. This leads to

$$E_{\text{roll}} = \left(\frac{2916 \pi^8 \gamma^5 a_0^4}{\mathcal{E}^2} \right)^{1/3}, \quad (\text{A4})$$

where we adopt for ice $\gamma = 7.3 \times 10^{-2} \text{ J m}^{-2}$ and $\mathcal{E} = 9.4 \text{ GPa}$ (Yamamoto et al. 2014).

In this Appendix, we explain how we extend the Suyama et al. (2008) equation (A1) to make it continuous in Section A1 for the hit and stick regime (i.e. $E_{\text{kin}} \leq 3bE_{\text{roll}}$) and in Section A2 for the internal restructuring regime (i.e. $E_{\text{kin}} \geq 3bE_{\text{roll}}$). It is equivalent to express ϕ_f as a power law of the grain mass m and quantities

of the disc. To do so, we chose to approximate E_{kin} as either very small or very large compared to E_{roll} in order to do a finite expansion. More detailed calculations leading to the equations presented in this Appendix can be found in Garcia (2018, in French).

A1 Hit-and-stick regime

If we consider $E_{\text{kin}} \ll E_{\text{roll}}$, equation (A1) becomes

$$\phi_f = \frac{2}{2.99} \phi_i. \quad (\text{A5})$$

Thus, we see that the filling factor in the hit-and-stick regime evolves as a geometrical progression with a common ratio $2/2.99$. We can express the filling factor ϕ_f of a grain with a mass m as a function of the monomer filling factor ϕ_0 and n the number of collisions to form that grain

$$\phi_f = \phi_0 \left(\frac{2}{2.99} \right)^n. \quad (\text{A6})$$

After one collision, the grain mass doubles. So after n collisions from a monomer, $m = 2^n m_0$. Consequently, the filling factor ϕ_f in the hit-and-stick regime (thereafter renamed $\phi_{\text{h\&s}}$) can be given as a function of m

$$\phi_{\text{h\&s}} = \phi_0 \left(\frac{m}{m_0} \right)^{\ln(2/2.99)/\ln(2)}. \quad (\text{A7})$$

Since monomers are compact, $\phi_0 = 1$. Note that we no longer have the recursive aspect of equation (A1).

A2 Internal restructuring regime

We consider here that $E_{\text{kin}} \gg E_{\text{roll}}$. Using $N_{\text{tot}} = 2m_i/m_0$ and $V_i/V_0 = 1/\phi_i (m_i/m_0)$, equation (A1) becomes

$$\phi_f = 2^{-1/5} \phi_i \left[1 + \frac{(3/5)^5 E_{\text{kin}}}{2bE_{\text{roll}}} \frac{1}{\phi_i^{10/3}} \left(\frac{m_i}{m_0} \right)^{-5/3} \right]^{3/10}. \quad (\text{A8})$$

However, E_{kin} depends on ϕ_i through v_{rel}^2 and the Stokes number St . Nevertheless, v_{rel}^2 does not vary linearly with the Stokes number. We consider $St \ll 1$ (resp. $St \gg 1$) in order to have $E_{\text{kin}} \propto St$ (resp. St^{-1}). With this approximation, ϕ_f is then related to ϕ_i at a certain power. The power depends on the grain drag regime (Epstein or Stokes) and if its Stokes number is smaller or larger than 1. As we want to express ϕ_f as $\phi_f \propto m^k$ with $k \in \mathbb{R}$, we have for given disc quantities, $\phi_f = 2^k \phi_i$. We define $\beta = 2^{-k}$, and thus $\phi_i = \beta \phi_f$. The values of β are different in Epstein and Stokes regimes and are taken to fit Eq. (A1) as discussed in Sections A2.1 and A2.2.

A2.1 In the Epstein regime and $St < 1$

In the Epstein regime with $St < 1$, the filling factor ϕ_f (thereafter renamed $\phi_{\text{Ep-St}<1}$) of a grain with mass m can be expressed as

$$\phi_{\text{Ep-St}<1} = \left(2^{1/5} - \beta_{\text{Ep}} \right)^{-3/8} \beta_{\text{Ep}}^{-5/8} 2^{1/8} \times \left(\frac{3}{10} \frac{(3/5)^5 2^{3/2} \text{Ro} \alpha m_0 c_g \rho_s a_0 \Omega_K}{8 \rho_g b E_{\text{roll}}} \right)^{3/8} \left(\frac{m}{m_0} \right)^{-1/8}, \quad (\text{A9})$$

where β_{Ep} is the value of β in the Epstein regime. As $k = -1/8$, $\beta_{\text{Ep}} = 2^{1/8}$.

Table A1. Definitions of the transition masses.

Transition masses	Transition
M_1	beginning of the collisional compression in the Epstein regime with $St < 1$
M_2	beginning of the collisional compression in the Stokes regime with $St < 1$
M_3	transition from the Epstein regime to the Stokes regime with $St < 1$
M_4	transition from $St < 1$ to $St > 1$ in the Epstein regime
M_5	transition from $St < 1$ to $St > 1$ in the Stokes regime

A2.2 In the Stokes regime and $St < 1$

In the Stokes regime with $St < 1$, the filling factor ϕ_f (thereafter renamed $\phi_{St-St<1}$) of a grain with mass m can be expressed as

$$\phi_{St-St<1} = \left(2^{1/5} - \beta_{St}\right)^{-1/3} \beta_{St}^{-2/3} \times \left(\frac{3}{10} \frac{(3/5)^5 2^{3/2} \text{Ro} \alpha m_0 c_g^2 \rho_s a_0^2 \Omega_K}{36 \mu_g b E_{\text{roll}}}\right)^{1/3}, \quad (\text{A10})$$

where β_{St} is the value of β in the Stokes regime. Since $\phi_{St-St<1}$ does not depend on the mass, $\beta_{St} = 1$.

A2.3 In the Epstein and Stokes regimes and $St > 1$

When the Stokes number St becomes larger than unity, the right term in the bracket on equation (A8) can be negligible compared to 1. If $St = 1$ is reached for a mass M_4 (respectively M_5) in the Epstein (resp. Stokes), the filling factor in this regime $\phi_{Ep-St>1}$ (resp. $\phi_{St-St>1}$) is expressed as

$$\phi_{Ep-St>1} = \phi_{Ep-St<1}(M_4) \left(\frac{m}{M_4}\right)^{-1/5}, \quad (\text{A11})$$

$$\phi_{St-St>1} = \phi_{St-St<1}(M_5) \left(\frac{m}{M_5}\right)^{-1/5}, \quad (\text{A12})$$

where M_4 and M_5 are respectively given by equations (A16) and (A17).

A3 Transition masses

In order to know in which regime the grain is, we compare its mass m with the limit masses in every regime with the algorithm. The names of those transition masses are reported in Table A1. The transition masses M_1 to M_5 are given by

$$\frac{M_1}{m_0} = \left[\left(2^{1/5} - \beta_{Ep}\right)^{-3/8} \beta_{Ep}^{-5/8} 2^{1/8} \times \left(\frac{3}{10} \frac{(3/5)^5 2^{3/2} \text{Ro} \alpha m_0 c_g^2 \rho_s a_0^2 \Omega_K}{8 \rho_g b E_{\text{roll}}}\right)^{3/8}\right]^{\frac{1}{\frac{1}{8} + \frac{\ln(2/2.99)}{\ln(2)}}}, \quad (\text{A13})$$

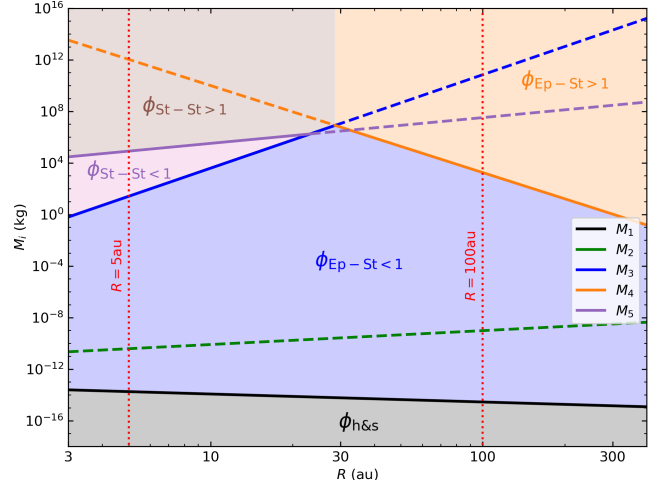


Figure A1. Different regimes of evolution of the filling factor encountered during collisions according to grain mass and distance from the star in the CTTS disc. Straight lines represent transitions between regimes. Dashed lines are used when transitions are no longer operating. The two vertical dotted red lines illustrate the regimes crossed by grains at 5 and 100 AU.

$$\frac{M_2}{m_0} = \left[\left(2^{1/5} - \beta_{St}\right)^{-1/3} \beta_{St}^{-2/3} \times \left(\frac{3}{10} \frac{(3/5)^5 2^{3/2} \text{Ro} \alpha m_0 c_g^2 \rho_s a_0^2 \Omega_K}{36 \mu_g b E_{\text{roll}}}\right)^{1/3}\right]^{\frac{\ln(2)}{\ln(2/2.99)}}, \quad (\text{A14})$$

$$\frac{M_3}{m_0} = \left(2^{1/5} - \beta_{St}\right)^{8/3} \left(2^{1/5} - \beta_{Ep}\right)^{-3} \beta_{St}^{16/3} \beta_{Ep}^{-5} 36^{8/3} 8^{-3} \times \left(\frac{3}{10} \frac{(3/5)^5 2^{3/2} \text{Ro} \alpha m_0 \rho_s \Omega_K}{b E_{\text{roll}}}\right)^{1/3} c_g^{-7/3} a_0^{-7/3} \rho_g^{-3} \mu_g^{8/3}, \quad (\text{A15})$$

$$\frac{M_4}{m_0} = \left(\frac{\rho_g c_g}{\Omega_K \rho_s a_0}\right)^4 2^{-1/3} \beta_{Ep}^{5/3} \left(2^{1/5} - \beta_{Ep}\right) \times \left(\frac{3}{10} \frac{(3/5)^5 2^{3/2} \text{Ro} \alpha m_0 c_g \rho_s a_0 \Omega_K}{8 \rho_g b E_{\text{roll}}}\right)^{-1}, \quad (\text{A16})$$

$$\frac{M_5}{m_0} = \left(\frac{9 \mu_g}{2 \Omega_K \rho_s a_0^2}\right)^{3/2} \beta_{St}^{1/3} \left(2^{1/5} - \beta_{St}\right)^{1/6} \times \left(\frac{3}{10} \frac{(3/5)^5 2^{3/2} \text{Ro} \alpha m_0 c_g^2 \rho_s a_0^2 \Omega_K}{36 \mu_g b E_{\text{roll}}}\right)^{-1/6}. \quad (\text{A17})$$

Note that those expressions depend only on the distance from the star R in the case of a power-law disc model.

The different transition masses are plotted in Fig. A1 for the CTTS disc. As shown in Figs. A1 and A2, all the dust begins to grow in the hit-and-stick regime before getting compacted by collisions in the Epstein drag regime. However, two different cases can be highlighted: grains in the first tens of AU transition to the Stokes regime as they grow while further in the disc, they keep growing in the Epstein regime. Moreover, Fig. A2 exhibits a comparison between the Suyama et al. (2008) discrete model and our continuous

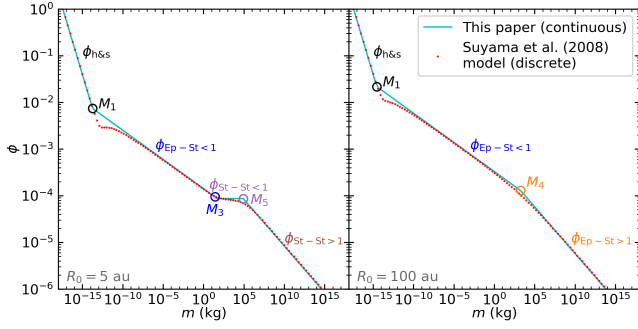


Figure A2. Comparison of our model of filling factor evolution during collisions (straight cyan lines) with the [Suyama et al. \(2008\)](#) discrete model (red dots) for grains evolving at fixed positions of 5 au (left) and 100 au (right) in the CTTS disc.

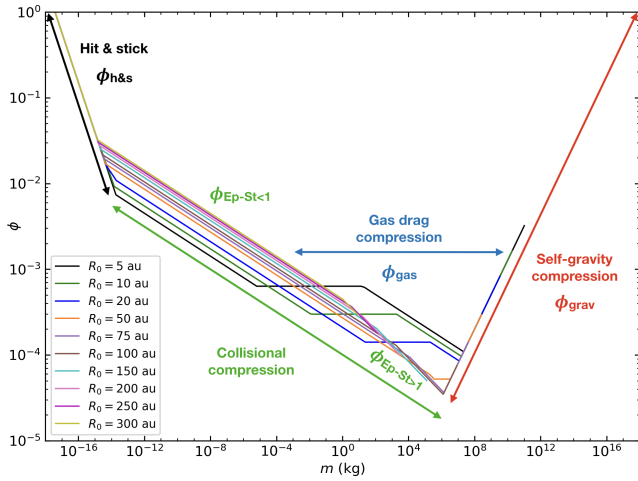


Figure B1. Grain filling factor as a function of mass in the CTTS disc at different fixed positions R_0 with the PACED code. Arrows show the different regimes encountered by the grains.

model. Both models mostly give similar results, allowing the simpler implementation of the continuous model in hydrodynamical codes. Our model deviates from that of [Suyama et al. \(2008\)](#) in two situations: for $E_{\text{cin}} \sim E_{\text{roll}}$ and $\text{St} \sim 1$. In both cases, the filling factor value we obtain is slightly higher than obtained with the discrete model but this difference is not significant for grains growth and dynamics and can be neglected.

A4 Algorithm

The algorithm allowing to compute the value of the filling factor after collisions ϕ_{col} is detailed in [Algorithm 1](#).

APPENDIX B: POROSITY EVOLUTION OF STATIC GRAINS IN THE FULL MODEL

[Figure B1](#) shows the evolution of the filling factor of static grains as they grow at different distances from the star as a function of their mass, computed with the PACED code. The different regimes in the collisional evolution (hit-and-stick and collisional compression) and static compression (gas drag and self-gravity) phases are

Algorithm 1 Calculation of ϕ_{col}

```

if  $M_2 < M_1$  then
  if  $m < M_2$  then
     $\phi_{\text{col}} = \phi_{\text{h\&s}}$ 
  else
    if  $m < M_5$  then
       $\phi_{\text{col}} = \phi_{\text{St-St}<1}$ 
    else
       $\phi_{\text{col}} = \phi_{\text{St-St}>1}$ 
    end if
  end if
else
  if  $m < M_1$  then
     $\phi_{\text{col}} = \phi_{\text{h\&s}}$ 
  else
    if  $M_4 > M_3$  then
      if  $m < M_3$  then
         $\phi_{\text{col}} = \phi_{\text{Ep-St}<1}$ 
      else
        if  $m < M_5$  then
           $\phi_{\text{col}} = \phi_{\text{St-St}<1}$ 
        else
           $\phi_{\text{col}} = \phi_{\text{St-St}>1}$ 
        end if
      end if
    else
      if  $m < M_4$  then
         $\phi_{\text{col}} = \phi_{\text{Ep-St}<1}$ 
      else
         $\phi_{\text{col}} = \phi_{\text{Ep-St}>1}$ 
      end if
    end if
  end if
end if
    
```

identified. [Figure B1](#) is to be compared with [Fig. 1](#), showing the porosity evolution of radially drifting grains (see [Section 3.1](#)).

This paper has been typeset from a \LaTeX file prepared by the author.